THE JOURNAL OF PHYSICAL CHEMISTRY A

 VOLUME 106, NUMBER 17, MAY 2, 2002

FEATURE ARTICLE

Allyl-A Model System for the Chemical Dynamics of Radicals

Ingo Fischer*,† and Peter Chen*,‡

Institut für Physikalische Chemie der Universität Würzburg, Am Hubland, D-97074 Würzburg, Lesezeichen, Germany, and Laboratorium für Organische Chemie der ETH Zürich, Universitätstrasse 16, CH-8092 Zürich, Switzerland

Received: October 3, 2001; In Final Form: January 8, 2002

The allyl radical, C_3H_5, is probably the currently best understood hydrocarbon radical. It is thus a model system for radical spectroscopy and dynamics. In this Feature Article we summarize the work performed on allyl in our laboratories by various laser spectroscopic techniques and develop a comprehensive picture of the processes occurring in allyl upon photoexcitation. This includes the structure of the excited electronic states of the neutral, as well as the ionic, ground state, the coupling phenomena between them, the primary photophysical processes directly after excitation, which occur on a picosecond time scale, and finally the unimolecular dissociation dynamics.

Introduction and Motivation

In this paper we will discuss the spectroscopy, structure, photochemistry and unimolecular reaction dynamics of the allyl radical, C_3H_5. It is presumably at present the best understood polyatomic radical, making it a benchmark molecule for investigations of radical dynamics.

Isolated hydrocarbon radicals play an important role in the chemistry of high energy environments, like combustion engines, hydrocarbon crackers, interstellar space or certain regions of the atmosphere. In fact, a large part of the chemistry of those systems is often determined by the dynamics of a few key radical species. It is thus no surprise that considerable effort is devoted to a detailed understanding of gas phase radical chemistry. Until recently the available technology limited the research to a few small (mostly di- or triatomic) systems. However, the technological progress in the development of both sources for the clean generation of radicals and new spectroscopic techniques applicable to short-lived species now permits detailed studies of radical structure and dynamics.

One class of key species are all hydrocarbons with a framework of three carbon atoms. They are assumed to be precursors in the formation of polycyclic aromatic hydrocarbons (PAH) and soot,[1] because the combination of two C_3 units gives access to the C_6 units important for the development of aromatic rings in one bimolecular step only. As soot is carcinogenic and damaging to engines, understanding its formation is one of the major challenges in combustion chemistry. Allyl itself is a particularly important intermediate in propane (C_3H_8), butane (C_4H_{10}) or acetylene-rich flames. It is formed from propene, C_3H_6, a primary product in propane flames, upon reactions with hydrogen atoms or OH radicals,[2,3] two species abundant in combustion processes. Data on the unimolecular dissociation of allyl are relevant because it is known that the predictions of kinetic models are sensitive to the rates of reactions that produce or consume hydrogen atoms.[4] Although allyl is stable in the ground state, it becomes reactive upon photochemical excitation at low energies as compared to stable molecules. Therefore one can assume that allyl radicals formed from partially unburned fuel also play a role as intermediates in tropospheric chemistry. Other work indicates its possible importance in interstellar chemistry.[5]

† Institut für Physikalische Chemie der Universität Würzburg. Fax: ++49-931/888-6378. E-mail: ingo@phys-chemie.uni-wuerzburg.de.

‡ Laboratorium für Organische Chemie der ETH Zürich. E-mail: chen@org.chem.ethz.ch.

10.1021/jp013708o CCC: $22.00
Published on Web 04/05/2002

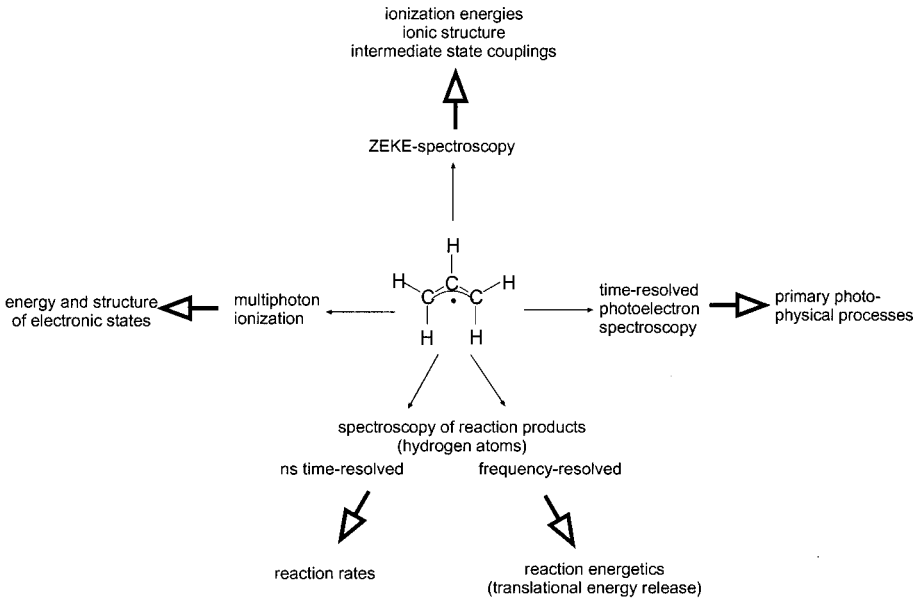

Figure 1. Overview on the various techniques applied to the allyl radical, and the information obtainable from the experiment.

Besides its practical relevance, allyl has numerous features that make it an interesting model for chemical dynamics in general:

·It possesses low lying excited electronic states with various degrees of vibronic couplings between them. This makes it an ideal compound to study nonadiabatic effects in molecules.

·Barriers to unimolecular reactions are low. Thus excitation with visible or near-ultraviolet light deposits enough energy to induce unimolecular reactions in these systems. Like in many radicals, the energetically and entropically most favorable unimolecular reaction channel in allyl is the loss of a hydrogen atom, because a closed-shell molecule is formed.

·Since several dissociation products are energetically close-lying, competing reaction channels exist. Loss of a hydrogen atom can lead to the formation of three different structural isomers with the composition C_3H_4. It is a challenge for chemical dynamics to sort the various channels according to their importance.

Although the dynamics of allyl shows a complexity comparable to that of much larger molecules, it is small enough to be studied by the sophisticated methods of laser spectroscopy. This makes it a perfect model systems to investigate chemical dynamics in general.

Experimental Section

Spectroscopic Techniques. It is our approach to choose the molecule first and then to select the techniques best suited to answer the relevant questions. To obtain a detailed understanding of the radical, the results of several experiments applying different laser spectroscopic methods have to be combined. Figure 1 summarizes the various techniques we utilized to investigate allyl and the information they yield.

All our experiments are performed in molecular beams in order to isolate the radical from its environment and to supress bimolecular reactions. One- and two-color multiphoton ionization (MPI) spectroscopy were applied to determine the structure and energies of the excited electronic states of allyl.[6,7] Structural information on the ion and an accurate ionization energy were derived from zero kinetic energy (ZEKE) photoelectron spectra, which also provided information on the structure of the intermediate electronic states and their couplings.[8]

As mentioned above, UV excitation of allyl deposits enough energy in the radical to trigger a unimolecular reaction. The early photophysical events following UV excitation were followed by means of time-resolved pump−probe photoelectron spectroscopy with picosecond time resolution.[9−11] The unimolecular dissociation itself occurred on a much longer nanosecond time scale. We investigated it by both time- and frequency-resolved detection of the reaction product, hydrogen atom.[12,13] While the nanosecond time-resolved experiments yielded reaction rates, the frequency-resolved experiments, yielding a Doppler profile of the H-atom, gave us information on the reaction energetics, including translational energy distributions.[14]

Due to the number of different techniques applied, we will restrict us to a short description of the detection schemes in the corresponding sub section. Information on the experimental details can be obtained from the publications cited in the text.

Generation of the Allyl Radical. The allyl radical is generated in a molecular beam by a technique called flash pyrolysis.[15] Two different precursors 1,5-hexadiene and allyl iodide, obtained commercially from Fluka and used without further purification, were employed. The precursor, seeded in 1−2 bar of helium, is expanded through a pulsed valve (0.8 mm orifice) with an electrically heated SiC tube of 1.0 mm diameter attached at the nozzle faceplate. The nozzle design has been described in the literature.[16,17] In the heated region the thermochemically weakest bond in the molecule is cleaved and the radical of interest is generated. Subsequent cooling in a supersonic expansion ensures that a beam of internally cold radicals is formed. Due to the short contact time of 10−50 μs between the molecules and the heated walls, the extent to which secondary fragmentation and bimolecular radical−radical recombinations can occur is limited. Number densities of more than 10^{14} radicals/cm^3 can be obtained at the nozzle exit, which typically yields around 10^{10} radicals/cm^3 in the interaction region of our spectrometers.

The Structure of the Allyl Radical

Allyl is an asymmetric rotor molecule belonging to the C_{2v} symmetry group. Conventionally, the principal axes of the molecule are defined in the way depicted in Figure 2. The allyl radical is oriented in the *yz*-plane, with the *z*-axis taken as the C_2-axis. The molecule-fixed axes *a*, *b*, and *c*, defined according

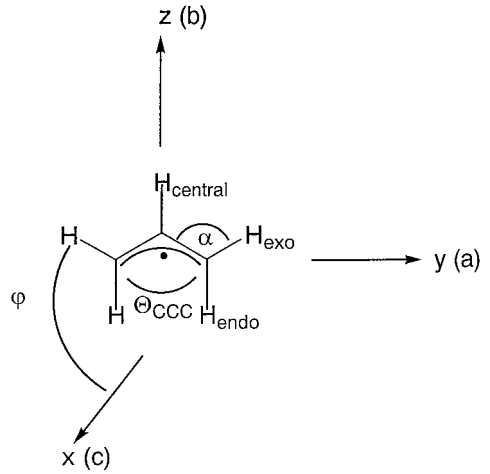

Figure 2. Orientation of the allyl radical in a Cartesian coordinate system and labeling of the atoms and geometry parameters. The angle φ indicates the angle of the terminal $-CH_2$ groups relative to the yz-plane.

TABLE 1: Geometry Parameters for Several Electronic States of the Allyl Radical (Values Taken from Calculations Given in Italics)

parameter	X $^2A_2$	B $^2A_1$ 0_0^0 [c]	C $^2B_1$ 0_0^0 [c]	X^+ $^1A_1$ [d]
r(C−$H_{central}$) (Å)	*1.087*[b]			*1.080*
r(C−H_{endo}) (Å)	*1.082*[b]			*1.082*
r(C−H_{exo}) (Å)	*1.085*[b]			*1.084*
r(C−C) (Å)	1.3869[a]	1.40	1.385	1.37
Θ(CCC) (deg)	123.96[a]	112	116.5	116.0
α(CCH_{endo}) (deg)	*121.5*[b]			*120.8*
α(CCH_{exo}) (deg)	*121.2*[b]			*121.7*
φ(dihedral) (deg)	0	20	0	0

[a] Reference 18. [b] Reference 21. [c] Reference 6. [d] Reference 10.

to an increasing moment of inertia $I_a < I_b < I_c$, are identified with the space fixed axes *y*, *z*, and *x*, corresponding to the Mulliken II^r notation. There are three distinguishable types of H-atoms present, labeled $H_{central}$, H_{exo} and H_{endo}, as depicted in the figure. In addition to the CCC bond angle Θ_{CCC} and the angle α ($CCH_{exo/endo}$), the angle φ is indicated in the figure, describing the position of the terminal methylene groups with respect to the *yz*-plane defined by the three carbon atoms.

The geometry of the $^2A_2$ electronic ground state was determined with high accuracy in several high-resolution experiments by IR laser spectroscopy on the ν_{11}, ν_1, and ν_{13} fundamentals.[18−20] The rotational constants were determined to be $A = 1.801890$ cm^{-1}, $B = 0.346320$ cm^{-1}, and $C = 0.290219$ cm^{-1}, indicating that allyl can be approximately treated as a near-prolate symmetric top with $\kappa \approx -0.9$. The C_{2v} symmetry was confirmed by the intensity variation of the rotational transitions apparent in the spectra due to nuclear spin statistics. With the aid of ab initio calculations[21] the bond lengths and angles were deduced from IR diode laser absorption measurements.[18] These values are given in the first column of Table 1. Information on the vibrational frequencies of the other modes in the ground state is available from resonance Raman spectroscopy,[22] IR spectroscopy in argon matrixes,[23,24] MPI spectroscopy,[6] and ab initio calculations.[25,26] They are summarized in the first column of Table 2.

Excited Electronic States. The energies of the low-lying excited electronic states of allyl, as well as the molecular orbitals of the π-system, are given in Figure 3. In contrast to the ground state, much less is known about the A $^2B_1$ state, which corresponds to a $\pi \rightarrow$ n transition. The bands in the original absorption spectrum, starting at 3.07 eV,[27] are not assigned; thus

TABLE 2: Vibrational Frequencies for Several Electronic States of the Allyl Radical (Values Taken from Computations Given in Italics)

	mode	X $^2A_2$	B $^2A_1$ [d]	C $^2B_1$ [d]	X^+ $^1A_1$ [h]
a_1	ν_1 as CH_2-stretch (in phase)	3113.98[a]			*3153*
	ν_2 CH-stretch	3052[b]			*3152*
	ν_3 sym CH_2-stretch	3027[b]			*3039*
	ν_4 sym CH_2 scissors	1478[b]			*1506*
	ν_5 sym CH_2 rock	1242[b]		1145	1239
	ν_6 CCC-stretch	1068[c]		1019	1027
	ν_7 CCC-bend	443[d]	379	385	431
a_2	ν_8 as CH_2 out of plane bend	775[b]	680[h]		*1080*
	ν_9 as CH_2 twist	*547*[e]	596		612
b_1	ν_{10} CH out of plane bend	983[b]	840		1078
	ν_{11} sym CH_2 out of plane bend	802[f]	1089		*972*
	ν_{12} sym CH_2 twist	522[d]	572		274
b_2	ν_{13} as CH_2-stretch	3110.60[a]			*3152*
	ν_{14} as CH-stretch	3020[b,g]			*3040*
	ν_{15} as CH_2 scissors	1463[b,g]			*1594*
	ν_{16} CH bend	1389[b,g]			*1406*
	ν_{17} as CCC-stretch	1182[b]	1261		1236
	ν_{18} as CH_2 rock	*913*[e]	952[h]		*922*

[a] Reference 20 (laser-diode spectroscopy). [b] Reference 24 (IR in Ar-matrix). [c] Reference 22 (resonance Raman). [d] Reference 6 and 33 (MPI). [e] Reference 26. [f] Reference 18 (laser-diode spectroscopy). [g] Reference 23 (IR in Ar-matrix). [h] Reference 8.

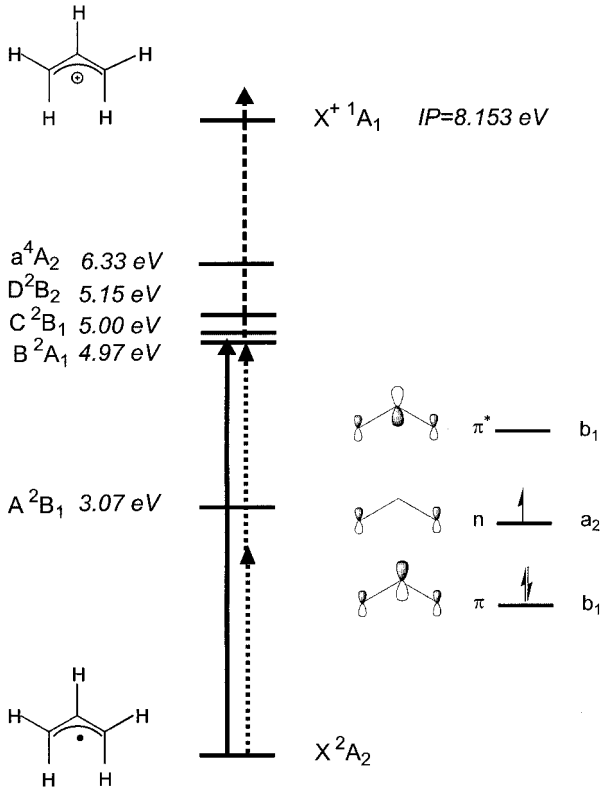

Figure 3. Location of the electronic states of the allyl radical. The UV bands of allyl between 4.99 and 5.21 eV can be excited either by one- (full arrow) or two-photon (dotted arrow) excitation. In many experiments ionization was performed by a different color (dashed arrow). The molecular orbitals of the π-system and their respective symmetry are depicted on the right-hand side of the figure.

the exact location of the origin is unclear. The location of the bands was recently confirmed in time-resolved experiments,[11] as well as in a cavity ring down study.[28] Ab initio calculations place the A-state at 3.13[29]and 3.19 eV,[30] respectively.

We focus predominantly on the UV band system starting at 250 nm. In the first absorption experiment[31] a number of bands were identified, but not assigned, the strongest ones being around

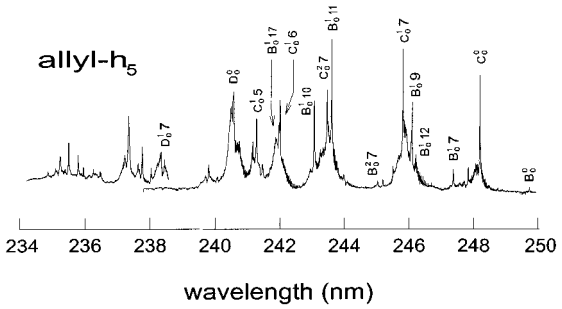

Figure 4. [1+1] survey scan of C_3H_5. Assignments are given as [state$_{\nu''}\nu'$ mode]. Reprinted from ref 6 by permission, copyright 1992, American Chemical Society.

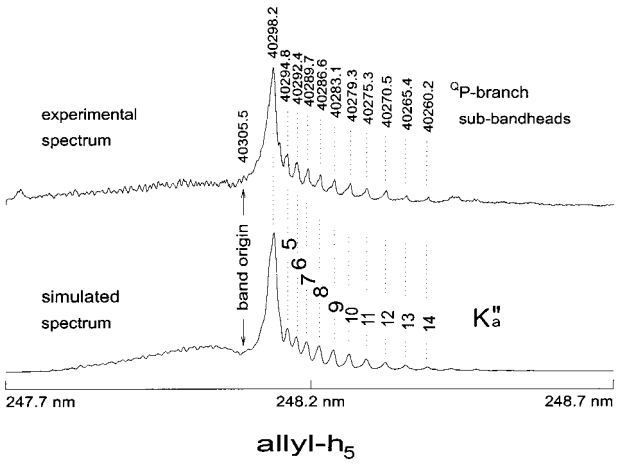

Figure 5. High-resolution scan over the C 0_0^0 band region of C_3H_5 (upper trace) with a rotational contour simulation as a type A band ($\Delta K = 0$) given in the lower trace. The spectrum was taken from ref 6 by permission, copyright 1992, American Chemical Society.

224 nm. Although a high oscillator strength of 0.23−0.26 was calculated for one of the electronic transitions,[29] and experimentally confirmed,[32] no fluorescence was reported, indicating short lifetimes. The relative location of the electronic states (B-, C-, and D-state) was determined in the [2+2] and [1+1] MPI experiments performed in our group.[6,7,33] Earlier [2+2] MPI studies[34,35] yielded only bands assigned to the B $^2A_1$ state, formally a 3s Rydberg state, symmetry-forbidden in a one-photon excitation from the electronic ground state. The C $^2B_1$ state, on the other hand, is formally a valence state, corresponding to a n → π^* transition, although it was computed to have considerable Rydberg character.[30] Figure 4 gives a [1+1] survey scan from 234 to 250 nm. The most notable features are the proximity of the B- and C-state origin (ΔE = 249 cm^{-1}) and the appearance of several formally symmetry-forbidden vibronic bands assigned to the B-state. Since this indicates a strong mixing of the states, the labels should be regarded as zero-order assignments only. Interestingly, the signal rapidly decreases to the blue of 240 nm, although the absorption cross section continues to increase.

The assignments given in Figure 4 are based on high-resolution scans of the bands, yielding a partially resolved rotational structure that permitted rotational band contour simulations. As an example, a high-resolution scan of the C-state origin band C 0_0^0, with a spectral resolution of around 1 cm^{-1}, is given in the upper trace of Figure 5, with a simulation shown for comparison in the lower trace. As mentioned, allyl can be regarded as a near-prolate top, permitting to label transitions according to the approximate quantum number K_a. The $^{\Delta K}\Delta J$ labeling scheme was employed to assign the transitions; thus the spectrum shows the P-branch of a type A band with the associated selection rule $\Delta K = 0$. As visible in the figure, the K-structure is well resolved for higher K_a'' quantum numbers. Each of the bands consists of a number of ΔJ transitions that could not be resolved with the lasers employed in the experiments. The extended rotational structure of the band indicates a significantly different rotational constant A in the excited state.

The simulations were performed using the ASYROT-PC program.[36] The rotational contour simulations yielded the symmetry of the excited-state vibronic bands, because each vibronic symmetry is associated with a given orientation of the transition dipole moment μ_T. A transition moment oriented along the *x*-axis leads to a type C band, associated with B_2 vibronic symmetry in the excited state. From type A ($\mu_T = y$) and type B ($\mu_T = z$) bands B_1 and A_1 vibronic symmetry can be deduced. Leaving all other parameters at their ground-state value, the CCC bond angle Θ_{CCC} and the CC bond length r_{C-C} were varied in the simulations until the peak positions and intensities were represented well. From the simulations the parameters Θ_{CCC} = 116.5 ± 1° and r_{C-C} = 1.385 ± 0.01 Å were obtained for the C-state origin. The reliability of these values was tested in experiments on the isotopomers of allyl,[33] C_3D_5, C_3HD_4, and C_3H_4D. Due to the reduction in Θ_{CCC} upon excitation, significant activity in the CCC bending mode ν_7' is present in all of the excited states, as visible in Figure 4.

A number of other bands were successfully fitted in a similar way. However, the two-parameter fit proved to be insufficient for the B-state origin. The B 0_0^0 state seems to be nonplanar, with the CH_2 groups rotated out of plane by a dihedral angle of $\varphi = 20°$. This indicates that the B-state, although formally a 3s Rydberg state, is significantly perturbed by the nearby valence states. For the other parameters values of Θ_{CCC} = 112° and r_{CC} = 1.40 Å were determined. The nonplanarity with the associated symmetry reduction also explains the appearance of the B 0_0^0 band and the totally symmetric ν_7' in the one-photon MPI spectrum, despite being formally forbidden in the C_{2v} point group. In addition, several nontotally symmetric modes of the B-state appear in the one-photon spectrum. Most of them (ν_{10}, ν_{11}, ν_{12}) are of b_1 symmetry and thus able to interact with the C-state origin, gaining oscillator strength through vibronic coupling. The most likely candidate for coupling the B- and the C-state through vibronic interaction is the ν_{12}' normal mode, corresponding to a symmetric CH_2 twist.[33] The geometry parameters and vibrational frequencies of the excited electronic states deduced from the spectra are summarized in Tables 1 and 2.

In addition to the states discussed here, several higher-lying states of allyl have been identified in the 6−8 eV energy range by [2+1] resonant MPI and assigned to a 3d and four *n*s (n = 4, 6−8) Rydberg states.[37] The progression in the CCC bending mode ν_7' was also apparent.

ZEKE Spectroscopy of the Allyl Cation. Photoelectron spectra of radicals are of considerable importance since many thermochemical properties, like binding energies, can be derived from the ionization energy through Born−Haber type cycles.[38] In addition, the spectra yield vibrational frequencies of the cation, thus allowing one to extract features of the potential energy surface of the cation. The limitations of conventional photoelectron spectroscopy (PES), like its inherently low resolution and its high sensitivity to stray fields, can now be overcome by the application of zero kinetic energy spectroscopy, ZEKE-PES, a technique based on the field ionization of very high-lying Rydberg states.[39,40] For most practical purposes, ZEKE-PES yields the same information as conventional PES,

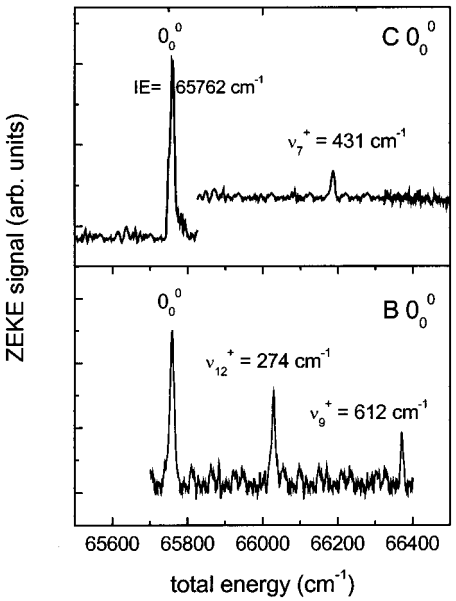

Figure 6. Zero kinetic energy photoelectron spectra of allyl obtained by [1+1′] excitation through the C 0_0^0 state (upper trace) dominated by the transition to the ionic origin and showing little vibrational activity. The spectrum obtained by [2+1′] excitation through the B 0_0^0 state (lower trace), on the other hand, shows significant activity in the modes corresponding to motion of the $-CH_2$ units out of the molecular plane, indicating a nonplanar geometry of the B 0_0^0.

but at an energy resolution of a few cm^{-1}, permitting one to resolve low-frequency vibrational and, at least for small molecules, even rotational states in the cation.

We recorded ZEKE spectra by means of either [1+1′] or [2+1′] excitation through selected intermediate vibronic states,[8] despite their short lifetimes (see below). The second laser excited allyl to high-lying Rydberg states, a few wavenumbers below the ionization limit. These states were field ionized by a −30 V/cm pulse applied after a field free delay time of 1.2 μs. During the delay time all kinetic electrons formed by direct ionization have disappeared from the interaction region.

Since the ionic ground state was computed to have a geometry similar to the C-state,[10,41] rather simple [1+1′] ZEKE spectra are expected within a Franck−Condon picture. As an example, the spectrum obtained through the C-state origin, C 0_0^0, is given in the upper trace of Figure 6. It is dominated by one peak corresponding to the transition to the ionic origin, $X^+\,^1A_1$ ($v^+ = 0$) ← C $^2B_1$ ($v' = 0$), yielding an ionization energy (IE) of 65762 ± 5 cm^{-1} or 8.153 eV. This value is in good agreement with earlier IE's of 8.15 eV[42] and 8.13 eV,[10] measured in conventional photoelectron spectra. However, a somewhat lower value of 8.12 eV was recently reported from an extrapolation of the s-Rydberg series.[37]

The simplicity of the spectrum confirms the similarity of geometries. Only one other peak is visible, at +431 cm^{-1}, corresponding to the ν_7^+ fundamental, the CCC bending mode. It appears due to a small reduction in the bending angle Θ_{CCC} upon ionization. In a similar manner ZEKE spectra were recorded through a number of intermediate states. Most of them were dominated by one or two bands, rendering an assignment of the cationic frequencies straightforward. The values are also given in Table 2. For the modes not observed experimentally the ab initio frequencies are listed in Table 2. The deviations between calculated and measured values were typically around 3%.

However, one ZEKE spectrum was not as simple to interpret: The spectrum obtained in a [2+1′] process through the B-state origin, B 0_0^0, depicted in the lower trace of Figure 6, showed considerable activity in low-frequency modes at +274 and + 612 cm^{-1}. By comparison with the computations, the two modes were assigned to the ν_{12}^+ and ν_9^+ fundamentals, corresponding to disrotatory and conrotatory motion of the $-CH_2$ groups out of the molecular plane. Within a Franck−Condon picture the high intensity indicates a geometry change along the two coordinates upon ionization. It thus provides an independent confirmation of the nonplanar geometry of the B-state origin and the strong mixing of states that was already evident from the MPI spectra. A double minimum potential appears along both coordinates, ν_9^+ and ν_{12}^+, as a consequence of vibronic interaction between the close-lying electronic states. The interaction between the B $^2A_1$ state and the C $^2B_1$ state, only 249 cm^{-1} higher in energy, is mediated by a mode of b_1 symmetry, like the ν_{12}, leading to a geometry distortion of the lower of the two coupled states. Due to the similarity with the Jahn−Teller effect this type of strong vibronic interaction is often termed the pseudo Jahn−Teller effect.[43] The double minimum potential along the ν_9 mode of a_2 symmetry is most likely due to a three-state interaction of the B-state with both C $^2B_1$ and D $^2B_2$.

Primary Photophysical Processes

The decrease of the MPI signal around 240 nm, despite the growing oscillator strength, indicates a fast nonradiative decay of the UV bands. On the other hand, from the resolution of approximately 1 cm^{-1} observed in the nanosecond experiments, a lower limit of 5 ps can be deduced for the lifetimes of these states. Earlier experiments addressing the dynamics upon UV excitation were ambiguous. While irradiation in an Ar-matrix yielded a mixture of allene, propyne, acetylene, methane, and traces of propene,[44] irradiation at 400 nm supposedly yielded the cyclopropyl radical.[45] Theoretical studies[46] suggested a disrotatory photocyclization upon UV excitation, a reaction pathway supported by a resonance Raman experiment at 224.63 nm.[22,47,48] We investigated the primary photophysical processes in allyl following UV excitation by picosecond time-resolved photoelectron spectroscopy (TR−PES), an excellent method to study nonradiative phenomena in isolated molecules, as discussed in the literature.[49,50] In our experiments a titanium: sapphire laser system was employed, regeneratively amplified at 10 Hz, delivering 2.5 ps, 6 mJ pulses at 400 nm. The details of the setup have been described previously,[10,11,51] including autocorrelation traces and frequency spectra.[51] The typical bandwidth was around 18 cm^{-1}, leading to a time-bandwidth product of 0.71, somewhat larger than the value of 0.44 for a perfect Gaussian pulse.

As shown elsewhere, the pump laser in our time-resolved pump−probe experiments excites individual UV vibronic bands of allyl.[11] The subsequent time evolution of the excited-state population is then monitored by a time-delayed probe pulse with sufficient energy to ionize allyl. Thus we obtain a time-dependent signal from the evolving intermediate state that is due to detection of electrons formed in the ionization process as a function of the pump−probe delay.

For all vibronic bands assigned in the spectrum given in Figure 4, photoelectron spectra were recorded every picosecond over a pump−probe delay range of around 100 ps.[10] A complete scan gives rise to a three-dimensional spectrum, like the one from the C-state origin, depicted in Figure 7. Here pulses with a wavelength of 248.1 and 274.3 nm for pump and probe, respectively, were employed, corresponding to a total energy of 9.52 eV. The photoelectron spectrum at the zero in time,

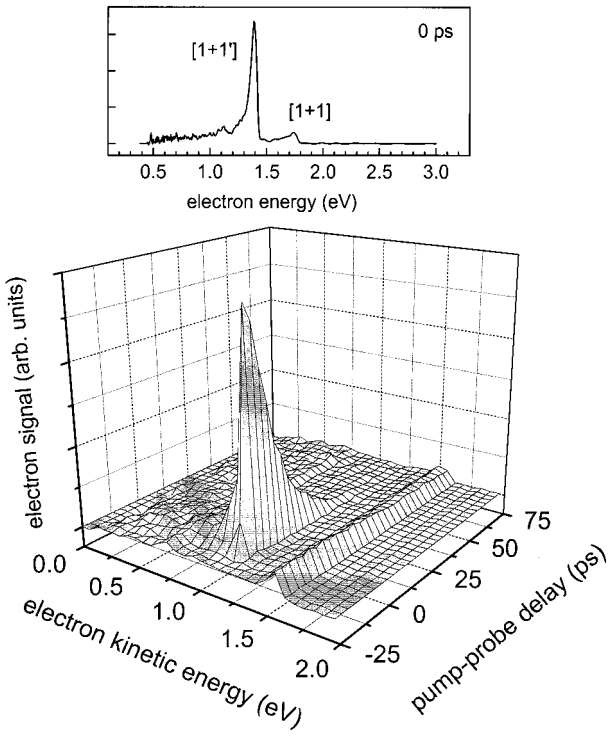

Figure 7. Complete time-resolved photoelectron spectrum from the C 0_0^0 state at 248.1 nm (taken from ref 10; reproduced with permission of American Institute of Physics, copyright 1998), with a one-dimensional slice showing the photoelectron spectrum at the zero in time in the upper trace. The time-dependent signal due to [1+1′] ionization, as well as a time-independent signal due to a [1+1] process can be recognized.

given in the upper trace of Figure 7 for the sake of illustration, was obtained from the full scan.

A sharp time-dependent peak due to [1+1′] ionization is visible at 1.37 eV electron excess energy. In addition, the pump laser alone can ionize the molecule in a [1+1] process, producing a time-independent background signal around 1.8 eV. As the excess energy transferred to the electron is different for the two processes, the signals associated with them appear at a different place in the photoelectron spectrum, allowing us to separate the time-dependent from the time-independent contributions. Photoelectron spectroscopy also permits the determination of the order of the time-dependent process from the electron energies, ensuring that the signal originates indeed from a [1+1′] process.

To obtain lifetimes, the intensity of the major time-dependent peak in the photoelectron spectrum was integrated and the integral plotted as a function of the pump−probe delay. This way a time constant of 15 ps was obtained for the population flow out of the C-state origin.

In the same manner lifetimes were obtained for the vibronic bands between 250 and 238 nm and for some bands beyond 238 nm detected before but not assigned.[10] An overall decrease of the lifetime with increasing excitation energy was observed, but no sudden jump is apparent. At the blue end of the energy range studied, the lifetime became as short as 5 ps around 236 nm. In the nanosecond MPI spectra the signal intensity for the vibronic transitions became rather small in this range, despite an absorption cross section that continues to grow down to 224 nm. Due to the decreasing lifetimes, ionization can no longer compete efficiently with the nonradiative decay of the states in experiments with nanosecond-laser pulses, leading to successively smaller signals in the nanosecond MPI experiments.

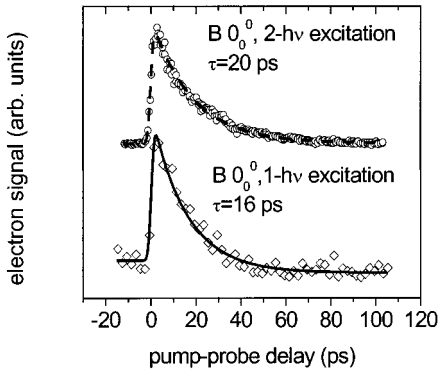

Figure 8. Due to the inversion doubling the B state origin splits into two components. The B 0_0^{0+} component can be excited in a two-photon process, while the B 0_0^{0-} component is only accessible by one-photon excitation. Thus individual lifetimes were obtained for the two components.

Again, particularly interesting results were obtained for the B-state origin. Pump−probe spectra of the B 0_0^0 state were recorded by both [1+1′] and [2+1′] excitation, with the lifetimes obtained depicted in Figure 8. Interestingly, different values of $\tau = 20$ ps (upper trace) and $\tau = 16$ ps (lower trace) were obtained upon [2+1′] and [1+1′] excitation, well beyond the experimental error bars of ±1 ps. This can be explained if the inverson doubling of the B-state origin in the double minimum potential is taken into account: The lower B 0_0^{0+} component with a_1 symmetry is accessible from the electronic ground state in a two-photon process, while the upper B 0_0^{0-} component with b_1 symmetry is only accessible in a one-photon process from the A_2 electronic ground state. Obviously, the splitting is too small to be observed in the frequency-domain spectrum. However, in the time-domain the two states can be distinguished by their lifetimes, once more confirming the double minimum potential of the B-state origin.

As discussed before[9−11] the decay of the UV states is attributed to internal conversion, IC. For this process two different pathways are possible, either decay directly to the ground state, or a two-step IC via the A state. To distinguish between the two, we will examine the factors contributing to the rate of nonradiative decay, $k_{i\rightarrow f}^{IC}$, within the framework of Fermi's Golden Rule[52]

$$k_{i\rightarrow f}^{IC} = \frac{2\pi}{\hbar}\langle M\rangle^2 \rho(E) \qquad (1)$$

The rate is governed by two factors, the density of states, $\rho(E)$, and the coupling matrix element M, which contains the wave function of the initial and final state of the IC process and the coupling operator H', according to

$$M = \langle \psi_i | H' | \psi_f \rangle \qquad (2)$$

Usually ψ_i and ψ_f are described by adiabatic wave functions, the nonadiabatic coupling being included in H'. In an often used approximation M is separated further into an electronic coupling matrix element β^{IC} and an overlap integral between the vibrational levels of the coupled states, $\langle \chi_i | \chi_f \rangle$, i.e., Franck−Condon factors. Here, however, the situation is more difficult: The initial state ψ_i, as discussed above, constitutes already a mixed state that cannot be adequately described by a single adiabatic wave function. Since it rather has to be expressed in terms of the B- and C-state electronic wave functions coupled by a vibrational mode, it cannot be separated further into an electronic and a vibrational part. From a theoretical point of

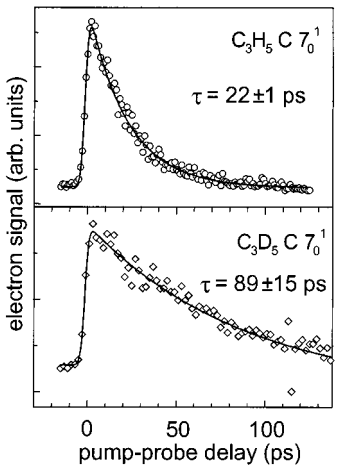

Figure 9. Lifetime measurements of the C 7_0^1 band of C_3D_5 (lower trace) showing an increase in lifetime from 22 to 89 ps as compared to C_3H_5 (upper trace). Reproduced from ref 11 by permission of the Royal Society of Chemistry, copyright 2000.

view a formally correct description of the nonradiative decay of the allyl UV bands requires the inclusion of at least four electronic states (still neglecting the D-state) and at least two vibrational modes and thus constitutes a rather challenging problem. We will therefore restrict ourselves to a more qualitative discussion. Since the vibrational density of states in the ground state at this energy is on the order of 10^{10} per cm^{-1} while the one for the A-state is more than 4 orders of magnitude smaller, the $\rho(E)$ term favors a direct conversion to the ground state. On the other hand, the magnitude of M typically scales inversely proportional to the energy gap between the two coupled electronic states. Conversion via the A-state should be favored by the smaller energy gap and a better overlap integral between the wave functions of the initial and the final state.

Information on the relative importance of the density of states and the coupling matrix element can be deduced from experiments on isotopic species. Deuteration of allyl should increase the density of states but lead to less favorable overlap integrals, because the C−D vibrations will less efficiently act as accepting modes as compared to the C−H vibrations. Thus the lifetimes of the C 7_0^1 bands of C_3H_5 and C_3D_5 were measured for comparison. As visible in Figure 9, the lifetime of this state increases by a factor of 4 upon deuteration. This indicates a nonradiative decay dominated by the coupling matrix element M and not by the density of states. Thus the primary photophysical decay is due to internal conversion from the UV bands to the A $^2B_1$ state.

Calculations indicate the presence of a conical intersection to the electronic ground state along the coordinate corresponding to cyclization,[11] although the upper state was not identified. The two intersections differ in the direction of twisting of the terminal $-CH_2$ groups: In one structure they are twisted in a conrotatory fashion, in the other one, in a disrotatory fashion. Thus, in our present picture, the internal conversion to the A-state within 20 ps or less is followed by a second decay to the electronic ground state through a conical intersection. Attempts to time-resolve the dynamics on the A-state surface were unsuccessful. Although a resonant enhancement of the pump−probe signal was observed[11] whenever one of the bands reported in absorption[27] was excited in the pump step, the observed decay was limited by the instrument response function. It is thus likely that the decay of the A-state through the conical intersection is very fast, and presumably occurs on a femtosecond time scale.

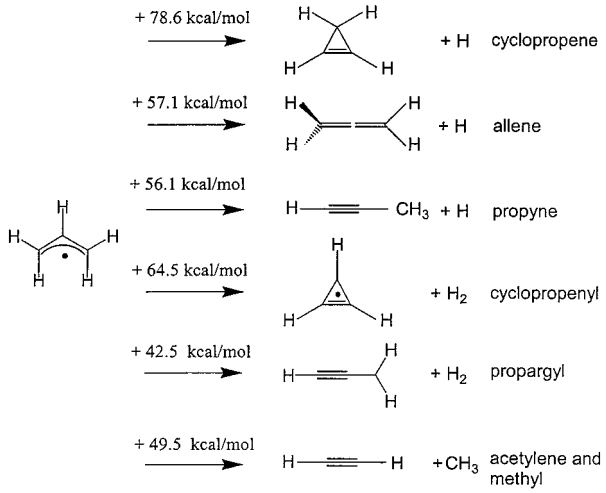

Figure 10. Possible reaction channels thermochemically accessible for the allyl radical at an energy of 115 kcal/mol, corresponding to excitation of the C 0_0^0 band at 248.15 nm together with their standard heats of formation relative to allyl. Reproduced from ref 11 by permission of the American Institute of Physics, copyright 1999.

Unimolecular Dissociation of the Allyl Radical

After the internal conversion following excitation to the C-state origin at 248.15 nm, an energy of 115 kcal/mol (481 kJ/mol) is deposited in the electronic ground state. At this excess energy several reaction channels are thermochemically accessible, as summarized in Figure 10. The values for the standard heats of formation relative to allyl are taken from the literature.[53−55] Three of the possible reactions are associated with loss of a hydrogen atom, leading to the formation of the C_3H_4 species cyclopropene, allene, and propyne. Two more channels, yielding cyclopropenyl or propargyl, are associated with the loss of H_2. Although formation of both C_3H_3 isomers is close in energy to the other channels, the loss of a hydrogen molecule generally proceeds via a high activation barrier and is thus considered unlikely. A sequential loss of two hydrogen atoms is thermochemically not possible at excitation energies around 5 eV.

Rupture of the C−C bond, yielding acetylene and a methyl radical, is also thermochemically possible because the products are only higher in energy by 49 kcal/mol (205 kJ/mol). However, this reaction requires two subsequent 1,2 hydrogen shifts before the C−C bond can break and is thus kinetically disfavored in comparison to hydrogen loss. Results of a recent investigation of this channel by photofragment translational spectroscopy[56] will be discussed below.

For the investigation of the unimolecular dissociation of hydrocarbon radicals, we detected hydrogen atoms by resonant MPI with nanosecond-lasers. The experimental scheme is depicted in Figure 11. A first nanosecond laser (solid arrow) excites allyl into the UV bands. The vibrationally hot radicals formed after internal conversion (IC) will dissociate after some time, preferentially by loss of a hydrogen atom. This atom is then detected with a second laser by resonant MPI via the ^2P-state (dashed and dotted arrows). This technique[57] is an extremely sensitive detection method, because of the very large cross-section of the 1s → 2p transition in atomic hydrogen at 121.6 nm (Lyman-α). Detection of the molecular fragments would be far more difficult, because all of them have the same mass, and the oscillator strength will be distributed over many rovibrational states.

Microcanonical reaction rates can be obtained from time-resolved detection of the H-atoms, while information on the

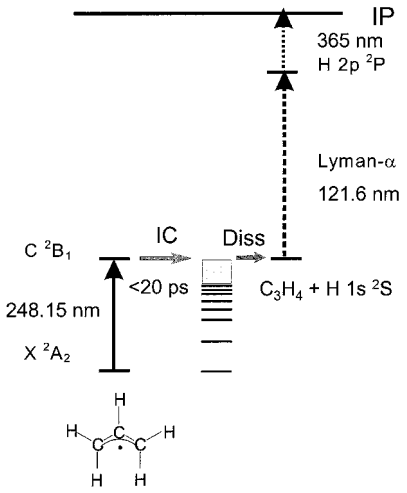

Figure 11. Schematic drawing of the nanosecond experiments. A first laser (solid arrow) excites allyl into the UV bands, which decay nonradiatively. Hot ground-state radicals are formed that dissociate into C_3H_4 and a H-atom, which is detected via the 1s → 2p transition. Note that 121.6 nm radiation (dashed arrow) is obtained by frequency-tripling of the 365 nm fundamental (dotted arrow).

reaction energetics can be gained from an analysis of the Doppler broadening of the hydrogen line.[58] The technique was applied to chemical problems by several groups[58−62] and is by now commonly used in experiments on elementary reaction dynamics.[63] While the majority of experiments was carried out in cells, with hydrogen detection performed via LIF, some experiments in molecular beams were also reported.[59,60,64] However, most of the work dealt with stable molecules.

Three types of experiments were performed: (1) The excitation laser was scanned in frequency with the detection laser fixed at the Lyman-α-wavelength in order to record resonant MPI spectra of allyl and action spectra of hydrogen, (2) the excitation laser was fixed to a UV transition of the allyl radical, while the detection laser was scanned across the hydrogen or deuterium absorption band in order to record Doppler profiles of the atomic reaction product (photofragment Doppler spectroscopy), and (3) both lasers were kept at a fixed frequency while the relative timing between the two was changed (i.e., time-resolved pump−probe spectra were recorded).

The type 1 experiments yielded signals in the H-atom action spectrum whenever a resonance in the allyl radical was excited, confirming that allyl loses an H-atom upon UV excitation.[13]

The observation of a hydrogen atom does not give us direct information on the molecular fragment formed in the dissociation process. However, such information can be obtained from isotopically labeled allyl radicals. Figure 12 shows the photofragment Doppler spectrum obtained from D_2CCHCD_2 radicals. As visible, this radical loses almost exclusively hydrogen (H/D ≈ 10/1), indicating that the central C−H bond is preferentially cleaved. Thus allene is the preferentially formed product! Cyclization would result in the loss of a terminal D-atom, while propyne formation should be associated with isotopic scrambling. The interpretation is supported by experiments on the isotopic mirror-image H_2CCDCH_2, which loses predominantly the D-atom.[12] Note that in the case of D_2CCHCD_2 the kinetic isotope effect works in favor of allene formation.

The Doppler profiles contain considerable information beyond just telling us whether H or D is lost in the reaction. When a molecule dissociates, a part of the excess energy is released as translational energy, E_T. Since the H-atom is light, it will carry away almost all of E_T and move out of the interaction region with considerable speed, leading to a broadening of the spectral

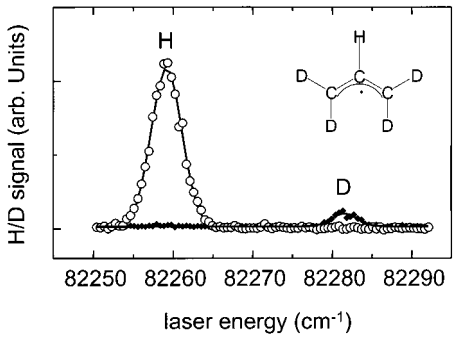

Figure 12. Photofragment Doppler spectroscopy of C_3HD_4 revealing H-loss, and thus cleavage of the central C−H bond, to be the dominant reaction channel. Thus allene is the preferentially formed product.

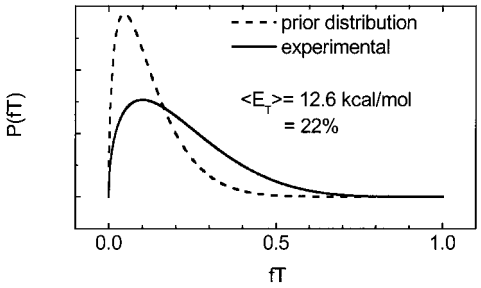

Figure 13. Translational energy distribution obtained from the Doppler profile. An expectation value of 12.6 kcal/mol is obtained; thus 22% of the excess energy in the reaction leading to allene is released into translation.

line due to the Doppler effect. From this line broadening a translational energy distribution, $P(E_T)$, can be obtained, giving the probability of a certain translational energy release taking place in the experiment.[14] For P the functional form

$$P(f_T) = f_T^{\,a} \times (1 - f_T^{\,b}) \tag{3}$$

was assumed,[65] with f_T being the fraction of excess energy released as translation and a and b being adjustable parameters. The Doppler profile can be fitted to this distribution function by optimizing a and b via an inversion procedure given in the literature.[14,66] The translational energy distribution obtained for allyl is given as solid line in Figure 13, together with the expectation value, $\langle E_T \rangle$, for the translational energy release. Assuming the formation of allene, around 22% of the excess energy is released as translation, within the range typical for statistical reactions. For comparison, the distribution derived from a simple statistical model, a prior distribution,[67] is given in the figure as a dotted line. It is peaked at smaller values of f_T than the experimental function. This discrepancy is most likely due to the reverse barrier for the H-loss of approximately 5 kcal/mol, which is not taken into account in a prior distribution. Recent models showed that this energy is predominantly released into translation.[68,69]

Although H-loss dominates, a small amount of D was also detected, indicating the presence of a second dissociation channel. Similar barriers were computed for allene formation and hydrogen migration to either the 2- or 1-propenyl radical,[13] but a significantly higher barrier was found for the formation of cyclopropene from cyclopropyl. H-loss from either of the two propenyl radicals can yield both allene and propyne. Due to the scrambling of H-atoms in the migration process no selectivity can be expected.

A time-resolved detection of the H-atoms yields the rate of appearance of the hydrogen, and thus microcanonical rates of the dissociation. As an example, the H signal versus the time

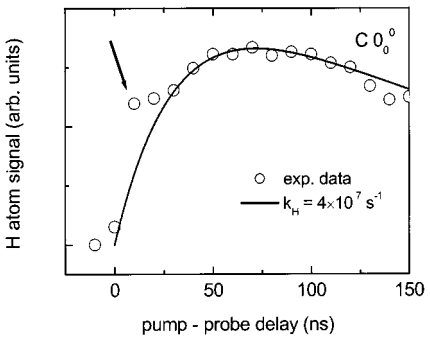

Figure 14. Appearance of the hydrogen signal as a function of time delay for initial excitation into the C 0_0^0 band. The solid line represents an exponential fit with a rate constant of $4 \times 10^7\ s^{-1}$. As the H-atom moves out of the line-of-sight, the signal decays at longer delay times. The earliest data point at 10 ns deviates from the fit, indicating the presence of a second process with an estimated rate of approximately $1 \times 10^8\ s^{-1}$.

delay between the two lasers upon excitation of the C 0_0^0 band is given in Figure 14. Note that the decay of the signal is due to the motion of H-atoms out of the observation region. Although the data could be fitted well by a rate of $4 \times 10^7\ s^{-1}$, two early data points deviate consistently from the fit. This observation constitutes evidence for a second process with a rate of $\approx 1 \times 10^8\ s^{-1}$ for the formation of H. It was confirmed by experiments on other bands of allyl, as well as the isotopomers. However, individual rates for two processes originating from the same educt can only be observed if one of the processes proceeds through an independent intermediate; otherwise the measured rate is just the sum of the two individual rates. Either the 1- or 2-propenyl radical, formed from allyl via hydrogen-shift, could constitute such an independent intermediate.

Figure 15 summarizes the unimolecular chemistry of the hot ground-state allyl. The dominant reaction channel is cleavage of the central C−H bond, resulting in the formation of allene. Presumably, the observed fast rate of $\approx 10^8\ s^{-1}$ is due to this reaction. Simple RRKM calculations[13] yielded a rate of $4 \times 10^8\ s^{-1}$ given in italics in the figure, which agrees reasonably well with the experimental rates. A second channel involves a hydrogen shift from allyl to either 1-propenyl or 2-propenyl. Both of these radicals can also lose hydrogen, also forming allene or propyne. This channel is associated with isotopic scrambling and thus responsible for the small deuterium signal in the photofragment Doppler spectrum of D_2CCHCD_2. We assume that the measured rate of $4 \times 10^7\ s^{-1}$ corresponds to this channel but cannot assign it to a particular rate determining step.

Translational energy spectroscopy, an alternative experimental approach, provides additional information. In this technique the translational energy of a photofragment is measured directly by its neutral time-of-flight. It works well for heavy fragments, but it is often difficult to analyze the loss of small fragments, like H, this way. Thus the technique is complementary to the optical detection of reaction products, which works best for small fragments, giving rise to large Doppler broadenings.

An investigation of allyl by translational energy spectroscopy[56] could not distinguish between the various isomeres of C_3H_4 but found a 16% contribution of the acetylene + methyl channel. The translational energy distribution of the methyl fragment peaked at a rather high energy of 20 kcal/mol, suggesting a large transition state barrier with respect to products. One would expect this reaction to proceed by two successive 1,2-H-shifts through the 1-propenyl intermediate, but

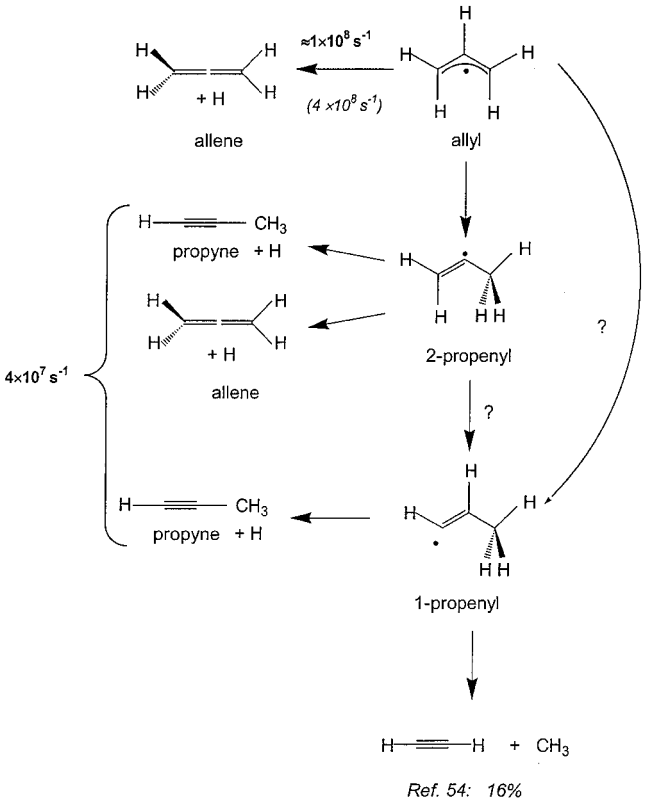

Figure 15. Summary of the unimolecular chemistry of the allyl radical at 115 kcal/mol. Two competing pathways, formation of allene and isomerization to 2-propenyl, can be observed. The experimental (bold) and RRKM (italics) rates are given. As is visible, allene formation is the dominating channel.

the barrier for a 1,2 H-shift from 2-propenyl to 1-propenyl was computed to be higher than the barrier to H-loss from 2-propenyl,[70] rendering this pathway unlikely. On the other hand the same group calculated the barrier for a 1,3 H-shift from allyl to 1-propenyl to be comparable to the barrier for the allyl/2-propenyl isomerization, so it might constitute a possible mechanism for the acetylene + methyl channel. It seems, however, that there are still open questions concerning the mechanism of C−C bond dissociation.

Other experiments aimed at the dynamics of the 2-propenyl itself. Mueller et al.[71,72] dispersed the products formed in the photodissociation of photolytically produced 2-propenyl by their translational energy, and subsequently ionized the C_3H_4 fragments by tunable VUV radiation. From the photoionization efficiency curves they concluded that propyne formation dominates the unimolecular chemistry of this radical.

Summary and Conclusion

This Feature Article gives a comprehensive picture of the structure and dynamics of allyl, one of the most important and by now best understood hydrocarbon radicals. It is demonstrated how detailed information on a complex system can be obtained from the combination of various laser-based spectroscopic techniques.

Like other unsaturated radicals allyl has a number of low-lying electronic states that exhibit nonadiabatic phenomena of various degrees. The UV states starting at 250 nm show strong vibronic coupling, leading to the geometry distortion of the B $^2A_1$ state (pseudo Jahn−Teller effect). Evidence for a double minimum potential along the coordinates corresponding to motion of the $-CH_2$ groups out of the molecular plane was obtained from MPI experiments, showing a number of sym-

metry-forbidden vibronic bands, from ZEKE experiments, showing a vibrational progression in the modes corresponding to this motion, and from time-resolved experiments, which yielded different lifetimes for the + and − component of the B-state origin that appear as a consequence of inversion doubling.

The primary photophysical processes upon UV excitation of allyl were elucidated by picosecond time-resolved photoelectron spectroscopy: The initially excited vibronic states decay in a two-step process: The first step is an internal conversion within 20 ps and less to the lower-lying A $^2B_1$ state, the second step is presumably a very fast decay from the A-state to the electronic ground state through a conical intersection.

In this process 5 eV (115 kcal/mol) of electronic energy are converted to internal energy, which is sufficient to overcome the barriers to several product channels. Photofragment Doppler spectroscopy of partially deuterated allyl showed cleavage of the central C−H bond, and thus formation of allene, to be the dominant reaction channel. In addition a 1,2 and/or 1,3 hydrogen shift occurs, leading to the formation of 1- and 2-propenyl radicals. This intermediate can lose a hydrogen atom to preferentially form propyne or undergo a C−C cleavage that leads to the formation of acetylene and methyl.

Acknowledgment. We thank all the students and postdocs involved in the work on allyl over the last couple of years, in order of appearance J. Blush, D. Minsek, H.-J. Deyerl, T. Schultz, and T. Gilbert. Financial support was provided by the National Science Foundation (U.S.A.), the Schweizerische Nationalfonds, the ETH Zürich, and the Fond der Chemischen Industrie (Germany).

References and Notes

(1) Marinov, N. M.; Castaldi, M. J.; Melius, C. F.; Tsang, W. *Combust. Sci. Technol.* **1997**, *128*, 295.
(2) Leung, K. M.; Lindstedt, R. P. *Combust. Flame* **1995**, *102*, 129.
(3) Thomas, S. D.; Bhargava, A.; Westmoreland, P. R.; Lindstedt, R. P.; Skevis, G. *Bull. Soc. Chim. Belg.* **1996**, *105*, 501.
(4) Miller, J. A.; Kee, R. J.; Westbrook, C. K. *Annu. Rev. Phys. Chem.* **1990**, *41*, 345−387.
(5) Webster, A. *Mon. Not. R. Astron. Soc.* **1993**, *265*, 421−30.
(6) Blush, J. A.; Minsek, D. W.; Chen, P. *J. Phys. Chem.* **1992**, *96*, 10150.
(7) Minsek, D. W.; Blush, J. A.; Chen, P. *J. Phys. Chem.* **1992**, *96*, 2025.
(8) Gilbert, T.; Fischer, I.; Chen, P. *J. Chem. Phys.* **2000**, *113*, 561−566.
(9) Schultz, T.; Fischer, I. *J. Chem. Phys.* **1997**, *107*, 8197.
(10) Schultz, T.; Fischer, I. *J. Chem. Phys.* **1998**, *109*, 5812.
(11) Schultz, T.; Clarke, J. S.; Deyerl, H.-J.; Gilbert, T.; Fischer, I. *Faraday Discuss.* **2000**, *115*, 17−31.
(12) Deyerl, H.-J.; Gilbert, T.; Fischer, I.; Chen, P. *J. Chem. Phys.* **1997**, *107*, 3329−2232.
(13) Deyerl, H.-J.; Fischer, I.; Chen, P. *J. Chem. Phys.* **1999**, *110*, 1450−1462.
(14) Kinsey, J. L. *J. Chem. Phys.* **1977**, *66*, 2560−2565.
(15) Chen, P.; Colson, S. D.; Chupka, W. A.; Berson, J. A. *J. Phys. Chem.* **1986**, *90*, 2319.
(16) Kohn, D. W.; Clauberg, H.; Chen, P. *Rev. Sci. Instrum.* **1992**, *63*, 4003−4005.
(17) Chen, P. In *Unimolecular and Bimolecular Reaction Dynamics*; Ng, C. Y., Baer, T., Powis, I., Eds.; Wiley: New York, 1994.
(18) Hirota, E.; Yamada, C.; Okunishi, M. *J. Chem. Phys.* **1992**, *97*, 2963.
(19) DeSain, J. D.; Thompson, R. I.; Sharma, S. D.; Curl, R. F. *J. Chem. Phys.* **1998**, *109*, 7803.
(20) Uy, D.; Davis, S.; Nesbitt, D. J. *J. Chem. Phys.* **1998**, *109*, 7793.
(21) Szalay, P. G.; Csaszar, A. G.; Fogarasi, G.; Karpfen, A.; Lischka, H. *J. Chem. Phys.* **1990**, *93*, 1246−1256.
(22) Getty, J. D.; Burmeister, M. J.; Westre, S. G.; Kelly, P. B. *J. Am. Chem. Soc.* **1991**, *113*, 801.
(23) Maier, G.; Reisenauer, H. P.; Rohde, B.; Dehnicke, K. *Chem. Ber.* **1983**, *116*, 732.
(24) Nandi, S.; Arnold, P. A.; Carpenter, B. K.; Nimlos, M. R.; Dayton, D. C.; Ellison, G. B. *J. Phys. Chem. A* **2001**, *105*, 7514−7524.
(25) Fjogstad, E.; Ystenes, M. *Spectrochim. Acta* **1990**, *46*A, 47−49.
(26) Sim, F.; Salahub, D. R.; Chin, S.; Dupuis, M. *J. Chem. Phys.* **1991**, *95*, 4317−4326.
(27) Currie, C. L.; Ramsay, D. A. *J. Chem. Phys.* **1966**, *45*, 488.
(28) Tonokura, K.; Koshi, M. *J. Phys. Chem.* **2000**, *104*, 8456−8461.
(29) Ha, T.-K.; Baumann, H.; Oth, J. F. M. *J. Chem. Phys.* **1986**, *85*, 1438.
(30) Oliva, J. M.; Gerratt, J.; Cooper, D. L.; Karadakov, P. B.; Raimondi, M. *J. Chem. Phys.* **1997**, *106*, 3663−3672.
(31) Callear, A. B.; Lee, H. K. *Trans. Faraday Soc.* **1968**, *64*, 308.
(32) Nakashima, N.; Yoshihara, K. *Laser Chem.* **1987**, *7*, 177.
(33) Minsek, D. W.; Chen, P. *J. Phys. Chem.* **1993**, *97*, 13375.
(34) Hudgens, J. W.; Dulcey, C. S. *J. Phys. Chem.* **1985**, *89*, 1505.
(35) Sappey, A. D.; Weisshaar, J. C. *J. Phys. Chem.* **1987**, *91*, 3731.
(36) Judge, R. H. *Comput. Phys. Commun.* **1987**, *47*, 361.
(37) Wu, J.-C.; Li, R.; Chang, J.-L.; Chen, Y.-T. *J. Chem. Phys.* **2000**, *113*, 7286−7291.
(38) Blush, J. A.; Clauberg, H.; Kohn, D. W.; Minsek, D. W.; Zhang, X.; Chen, P. *Acc. Chem. Res.* **1992**, *25*, 385.
(39) Müller-Dethlefs, K.; Schlag, E. W. *Annu. Rev. Phys. Chem.* **1991**, *42*, 109−136.
(40) Müller-Dethlefs, K.; Schlag, E. W. *Angew. Chem., Int. Ed. Engl.* **1998**, *37*, 1346−1374.
(41) Reindl, B.; Clark, T.; Schleyer, P. V. R. *J. Comput. Chem.* **1997**, *18*, 533−51.
(42) Houle, F. A.; Beauchamp, J. L. *J. Am. Chem. Soc.* **1978**, *100*, 3290.
(43) Fischer, G. *Vibronic Coupling*; Academic Press: London, 1984.
(44) Maier, G.; Senger, S. *Angew. Chem., Int. Ed. Engl.* **1994**, *33*, 558.
(45) Holtzhauer, K.; Cometta-Morini, C.; Oth, J. F. M. *J. Phys. Org. Chem.* **1990**, *3*, 219.
(46) Merlet, P.; Peyerimhoff, S. D.; Buenker, R. J.; Shih, S. *J. Am. Chem. Soc.* **1974**, *96*, 959.
(47) Getty, J. D.; Liu, X.; Kelly, P. B. *J. Phys. Chem.* **1992**, *96*, 10155.
(48) Getty, J. D.; Liu, X.; Kelly, P. B. *Chem. Phys. Lett.* **1993**, *201*, 236.
(49) Lochbrunner, S.; Larsen, J. J.; Shaffer, J. P.; Schmitt, M.; Schultz, T.; Underwood, J. G.; Stolow, A. *J. Electron Spectrosc.* **2000**, *112*, 183−198.
(50) Neumark, D. M. *Annu. Rev. Phys. Chem.* **2001**, *52*, 255−278.
(51) Fischer, I.; Schultz, T. *Appl. Phys. B: Lasers Opt.* **1997**, *64*, 15.
(52) Freed, K. F. *Acc. Chem. Res.* **1978**, *11*, 74−80.
(53) Chen, P. In *Unimolecular and Bimolecular Reaction Dynamics*; Ng, C. Y., Baer, T., Powis, I., Eds.; Wiley: New York, 1994; pp 371−425.
(54) Clauberg, H.; Minsek, D. W.; Chen, P. *J. Am. Chem. Soc.* **1992**, *114*, 99−107.
(55) *CRC Handbook of Chemistry and Physics*; Lide, D. A., Ed.; CRC: Boca Raton, FL, 1994.
(56) Stranges, D.; Stemmler, M.; Yang, X.; Chesko, J. D.; Suits, A. G.; Lee, Y. T. *J. Chem. Phys.* **1998**, *109*, 5372−5382.
(57) Zacharias, H.; Rottke, H.; Danon, J.; Welge, K.-H. *Opt. Commun.* **1981**, *37*, 15.
(58) Tsukiyama, K.; Bersohn, R. *J. Chem. Phys.* **1987**, *86*, 745.
(59) Schmiedl, R.; Dugan, H.; Meier, W.; Welge, K.-H. *Z. Phys. A* **1982**, *304*, 137.
(60) Koplitz, B.; Xu, Z.; Baugh, D.; Buelow, S.; Häusler, D.; Rice, J.; Reisler, H.; Quiang, C. X. W.; Noble, M.; Wittig, C. *Faraday Discuss. Chem. Soc.* **1986**, *82*, 125.
(61) Gerlach-Meyer, U.; Linnebach, E.; Kleinermanns, K.; Wolfrum, J. *Chem. Phys. Lett.* **1987**, *133*, 113.
(62) Park, J.; Bersohn, R.; Oref, I. *J. Chem. Phys.* **1990**, *93*, 5700.
(63) Volpp, H.-R.; Wolfrum, J. In *Gas-Phase Chemical Reaction Systems*; Wolfrum, J., Volpp, H.-R., Rannacher, R., Warnatz, J., Eds.; Springer: Berlin, 1996.
(64) Cromwell, E. F.; Stolow, A.; Vrakking, M. J. J.; Lee, Y. T. *J. Chem. Phys.* **1992**, *97*, 4029.
(65) We would like to thank S. N. North for valuable discussions on translational energy distributions
(66) He, Y.; Pochert, J.; Quack, M.; Ranz, R.; Seyfang, G. *Faraday Discuss.* **1995**, *102*, 275.
(67) Levine, R. D.; Bernstein, R. B. *Molecular Reaction Dynamics and Chemical Reactivity*; Oxford University Press: New York, 1987.
(68) North, S. W.; Blank, D. A.; Gezelter, J. D.; Longfellow, C. A.; Lee, Y. T. *J. Chem. Phys.* **1995**, *102*, 4447.
(69) Mordaunt, D. H.; Osborn, D. L.; Neumark, D. M. *J. Chem. Phys.* **1998**, *108*, 2448.
(70) Davis, S. G.; Law, C. K.; Wang, H. *J. Phys. Chem. A* **1999**, *103*, 5889−5899.
(71) Mueller, J. A.; Miller, J. L.; Butler, L. J.; Qi, F.; Sorkhabi, O.; Suits, A. G. *J. Phys. Chem. A* **2000**, *104*, 11261−11264.
(72) Mueller, J. A.; Parsons, B. F.; Butler, L. J.; Qi, F.; Sorkhabi, O.; Suits, A. G. *J. Chem. Phys.* **2001**, *114*, 4505−4521.